

Magnetic properties of $\text{Co}_c\text{Mn}_{1-c}\text{Cl}_2\text{-FeCl}_3$ graphite bi-intercalation compounds

Itsuko S. Suzuki and Masatsugu Suzuki

Department of Physics, State University of New York at Binghamton, Binghamton, New York 13902-6000

(Received 14 November 1994)

$\text{Co}_c\text{Mn}_{1-c}\text{Cl}_2\text{-FeCl}_3$ graphite bi-intercalation compounds (GBIC's) form superlattices with a c -axis stacking sequence of $G_1G_2G_1G_2\dots$, where the $\text{Co}_c\text{Mn}_{1-c}\text{Cl}_2$ layer ($=I_1$) and FeCl_3 layer ($=I_2$) alternate with a single graphite layer ($=G$). We have studied the magnetic properties of these compounds by low-field superconducting quantum interference device (SQUID) magnetization, and ac and dc magnetic-susceptibility measurements. $\text{Co}_c\text{Mn}_{1-c}\text{Cl}_2\text{-FeCl}_3$ GBIC's with $0 \leq c \leq 0.1$ show a ferromagnetic behavior characterized by a positive Curie-Weiss temperature, an irreversible effect of SQUID magnetization, and a broad peak in the ac magnetic susceptibility. This ferromagnetic behavior can be explained in terms of either the ferromagnetic nearest-neighbor intraplanar exchange interaction of MnCl_2 layers, or a possible competition of Ising Fe^{2+} spins and XY Fe^{3+} spins in the FeCl_3 layers. For $0.25 \leq c \leq 0.7$ the antiferromagnetic phase occurs in the FeCl_3 layers. For $0.45 \leq c \leq 0.7$ this antiferromagnetic phase coexists with a spin-glass-like phase occurring in the $\text{Co}_c\text{Mn}_{1-c}\text{Cl}_2$ layers below a characteristic temperature T_0 (≈ 9 K). For $0.7 < c < 1$ there occurs a cluster glass phase below a critical temperature T_c in the $\text{Co}_c\text{Mn}_{1-c}\text{Cl}_2$ layers, where the spin directions of ferromagnetic clusters are frozen. The nature of this cluster glass phase is different from that for stage-2 $\text{Co}_c\text{Mn}_{1-c}\text{Cl}_2$ GIC's with $0.8 \leq c \leq 1$.

I. INTRODUCTION

The magnetic graphite bi-intercalation compounds (GBIC's) offer possibilities for the formation of superlattices with a stacking sequence of $G_1G_2G_1G_2\dots$ along the c axis. Two different intercalate layers (I_1 and I_2) alternate with a single graphite layer (G). The magnetic properties of magnetic GBIC's have attracted considerable attention,¹⁻⁹ partly because of the crossover behavior from two-dimensional (2D) to three-dimensional (3D). These compounds provide model systems for studying the magnetic phase transition associated with spin frustration effects arising from the competition among various kinds of intraplanar and interplanar exchange interactions. Recently we have prepared samples of $\text{Co}_c\text{Ni}_{1-c}\text{Cl}_2\text{-FeCl}_3$ GBIC's (Ref. 9) and $\text{Co}_c\text{Mn}_{1-c}\text{Cl}_2\text{-FeCl}_3$ GBIC's (Ref. 7) with well-defined c -axis stacking sequences by a method of sequential intercalation: $I_1 = \text{Co}_c\text{Ni}_{1-c}\text{Cl}_2$, $\text{Co}_c\text{Mn}_{1-c}\text{Cl}_2$ ($0 \leq c \leq 1$) and $I_2 = \text{FeCl}_3$. The I_1 -intercalate layer of these compounds is formed of two different magnetic ions which are randomly distributed on the triangular lattice. In the previous paper⁹ we have reported the magnetic properties of $\text{Co}_c\text{Ni}_{1-c}\text{Cl}_2\text{-FeCl}_3$ GBIC's. In these compounds the average intraplanar exchange interaction of the $\text{Co}_c\text{Ni}_{1-c}\text{Cl}_2$ layer is ferromagnetic and the intraplanar exchange interaction of the FeCl_3 layer is antiferromagnetic. The $\text{Co}_c\text{Ni}_{1-c}\text{Cl}_2$ layer undergoes a ferromagnetic phase transition at the critical temperature T_c which changes from 19.48 K at $c=0$ to 9.10 K at $c=1$. Near T_c the in-plane spin-correlation length of the $\text{Co}_c\text{Ni}_{1-c}\text{Cl}_2$ layer divergingly grows, leading to the 3D-like magnetic phase transition through an interplanar interaction enhanced by the intervening FeCl_3 layer. The

antiferromagnetic long-range order of the FeCl_3 layer around 3 K is smeared by the ferromagnetic long-range order of $\text{Co}_c\text{Ni}_{1-c}\text{Cl}_2$ layers. In spite of such complicated magnetic phase transitions in $\text{Co}_c\text{Ni}_{1-c}\text{Cl}_2\text{-FeCl}_3$ GBIC's, the nature of magnetic phase transitions in $\text{Co}_c\text{Ni}_{1-c}\text{Cl}_2\text{-FeCl}_3$ GBIC's seems to be independent of the Co concentration.

In the present paper we study the magnetic properties of $\text{Co}_c\text{Mn}_{1-c}\text{Cl}_2\text{-FeCl}_3$ GBIC's which are expected to be very different from those of $\text{Co}_c\text{Ni}_{1-c}\text{Cl}_2\text{-FeCl}_3$ GBIC's. In the $\text{Co}_c\text{Mn}_{1-c}\text{Cl}_2$ layer of $\text{Co}_c\text{Mn}_{1-c}\text{Cl}_2\text{-FeCl}_3$ GBIC's the average intraplanar exchange interaction is expected to change from ferromagnetic to antiferromagnetic with decreasing concentration c . The spin frustration effect arising from the competition between ferromagnetic and antiferromagnetic intraplanar exchange interactions may lead to a drastic change of the effective interplanar interaction between $\text{Co}_c\text{Mn}_{1-c}\text{Cl}_2$ and FeCl_3 layers. We report experimental results on (00L) x-ray scattering, low-field SQUID magnetization, and dc and ac magnetic susceptibility of $\text{Co}_c\text{Mn}_{1-c}\text{Cl}_2\text{-FeCl}_3$ GBIC's. We investigate the effect of the bi-intercalation on the magnetic phase transitions of $\text{Co}_c\text{Mn}_{1-c}\text{Cl}_2\text{-FeCl}_3$ GBIC's by comparing the experimental results of $\text{Co}_c\text{Mn}_{1-c}\text{Cl}_2\text{-FeCl}_3$ GBIC's with those of stage-2 $\text{Co}_c\text{Mn}_{1-c}\text{Cl}_2$ GIC's.¹⁰⁻¹²

II. BACKGROUND

A. Spin Hamiltonian of stage-2 MnCl_2 GIC

The stage-2 MnCl_2 GIC magnetically behaves like a quasi-2D XY-like spin system on the triangular lattice.¹³⁻¹⁷ This compound undergoes a magnetic phase

transition at the critical temperature $T_c = 1.1$ K.^{13,14} The Curie-Weiss temperature Θ and the effective magnetic moment P_{eff} are given by $\Theta = -5.94$ K and $P_{\text{eff}} = 5.83\mu_B$, respectively.¹⁵ The g factor is almost isotropic and given by $g_c = 1.912 \pm 0.005$ along the c axis and $g_a = 1.977 \pm 0.005$ along any direction perpendicular to the c axis.^{16,17} The electron-paramagnetic-resonance measurement of MnCl_2 GIC reveals that the anisotropy of g factor defined by $\Delta g (=g_a - g_c)$ begins to appear below 50 K, and becomes more pronounced below 30 K.^{16,17} This anisotropy of the g factor is identified as the onset of short-range spin order below 30 K. The heat capacity of the stage-2 MnCl_2 GIC shows no appreciable anomaly at T_c but exhibits a broad plateau between 5 and 10 K associated with the growth of 2D short-range spin order.¹⁴ The real part χ' of ac magnetic susceptibility has a peak at T_c .¹⁴ The remnant magnetization observed below T_c suggests a ferromagnetic behavior in MnCl_2 GIC.¹⁴

It has been believed that the spin Hamiltonian of Mn^{2+} ions in the stage-2 MnCl_2 GIC is described by¹⁵

$$H = -2J \sum_{\langle i,j \rangle} \mathbf{S}_i \cdot \mathbf{S}_j + D \sum_i (S_i^z)^2 - 2J' \sum_{\langle i,m \rangle} \mathbf{S}_i \cdot \mathbf{S}_m, \quad (1)$$

with spin $S = \frac{5}{2}$, where the z axis coincides with the c axis, D is the single-ion anisotropy ($D = 0.97$ K), J is the nearest-neighbor (NN) intraplanar antiferromagnetic interaction ($J = -0.20$ K), J' is an interplanar exchange interaction, and the summation is over nearest-neighbor intraplanar pairs i and j , and the nearest-neighbor interplanar pairs i and m . The single-ion anisotropy constant D is positive, indicating XY spin anisotropy. It is well known that for these XY spins all the neighboring spins cannot align antiparallel to each other so that a compromise has to be made to gain exchange energy, leading to the $\sqrt{3} \times \sqrt{3}$ spin structure, where the spins are rotated successively by 120° .^{18,19}

Recent elastic neutron scattering study shows the deviation of the in-plane spin structure of MnCl_2 GIC from the 120° spin structure.²⁰ The magnetic Bragg reflections are observed below 7.5 K at the in-plane wave vector $\mathbf{Q} = \{\mathbf{Q}_i \pm \mathbf{k}_i\}$, where \mathbf{Q}_i is the in-plane reciprocal-lattice vector of MnCl_2 layers and \mathbf{k}_i is the reciprocal-lattice vector of the in-plane spin structure: $|\mathbf{Q}_i| = 1.965 \text{ \AA}^{-1}$. The value of $|\mathbf{k}_i|$ is 0.522 \AA^{-1} below 0.43 K, increases with increasing temperature, and becomes almost constant (0.532 \AA^{-1}) above T_c . With further increasing temperature above 5 K the value of $|\mathbf{k}_i|$ approaches that of $2\sqrt{3} \times 2\sqrt{3}$ spin structure. This incommensurate $2\sqrt{3} \times 2\sqrt{3}$ -like spin structure can be realized when NN, and next-nearest-neighbor (NNN), . . . , exchange interactions are taken into account in the Fourier transform of a classical spin Hamiltonian. Note that the NNN exchange interaction J_1 should be antiferromagnetic and be on the same order as the ferromagnetic NN exchange interaction J_0 in magnitude. The spin frustration effect arising from the competing ferromagnetic and antiferromagnetic intraplanar exchange interactions gives rise to the incommensurate in-plane spin structure in MnCl_2 GIC.

B. Magnetic properties of stage-2 $\text{Co}_c\text{Mn}_{1-c}\text{Cl}_2$ GIC's (Refs. 10–12)

Stage-2 $\text{Co}_c\text{Mn}_{1-c}\text{Cl}_2$ GIC's are 2D random spin systems with competing intraplanar exchange interactions. The Co^{2+} and Mn^{2+} ions are distributed randomly in the same intercalate layer. The magnetic properties of these compounds have been studied by dc and ac magnetic susceptibility, and low-field superconducting quantum interference device (SQUID) magnetization.^{10–12} The Curie-Weiss temperature increases monotonically with increasing Co concentration. Its sign changes from negative to positive around $c \approx 0.2$, indicating that the average intraplanar exchange interaction is antiferromagnetic for $0 \leq c < 0.2$, and is ferromagnetic for $0.2 < c \leq 1$. These compounds show a magnetic phase transition between the paramagnetic phase to the ferromagnetic phase for $c \geq 0.45$. For $0.9 \leq c \leq 1$ where the intraplanar ferromagnetic interactions are dominant, a cluster glass phase appears below T_c . For $0.8 \leq c < 0.9$ where the antiferromagnetic intraplanar exchange interaction becomes comparable to the ferromagnetic intraplanar exchange interaction, a spin-glass-like phase appears below T_c .

The intraplanar exchange interactions between Co and Co, and Mn and Mn in stage-2 $\text{Co}_c\text{Mn}_{1-c}\text{Cl}_2$ GIC's are assumed to be the same as those in stage-2 CoCl_2 GIC's and stage-2 MnCl_2 GIC's, respectively.¹⁰ If the spin Hamiltonian of the stage-2 MnCl_2 GIC is given by Eq. (1), the intraplanar exchange interaction between Co^{2+} and Mn^{2+} spins for stage-2 $\text{Co}_c\text{Mn}_{1-c}\text{Cl}_2$ GIC's is found to be ferromagnetic and be described by $J(\text{Co-Mn}) = 1.2[J(\text{Co-Co})|J(\text{Mn-Mn})|]^{1/2} = 1.49$ K, with $J(\text{Co-Co}) = 7.75$ K and $J(\text{Mn-Mn}) = -0.2$ K. The effective magnetic moments of Co^{2+} are given by $P_{\text{eff}}(\text{Co}) = g(\text{Co}) [S(S+1)]^{1/2} = 5.54\mu_B$ for the g value $g(\text{Co}) = 6.40$ and fictitious spin $S = \frac{1}{2}$.

C. Magnetic properties of FeCl_3 GIC's

Many studies have been made on the stage-1 and stage-2 FeCl_3 GIC's, while very few studies have been made on the stage-1 and stage-2 FeCl_2 GIC's.^{21–25} The in-plane structure of the FeCl_3 layer in the FeCl_3 GIC's forms a honeycomb lattice, where there are two Fe atoms per unit cell with a lattice constant $a = 6.13 \text{ \AA}$. The FeCl_3 layer is incommensurate with the graphite layer. The primitive lattice vector of the FeCl_3 layer is rotated by 30° with respect to that of the graphite layer. The FeCl_3 GIC's magnetically behave like a quasi-2D XY -like antiferromagnet. The spin Hamiltonian for Fe^{3+} ions with spin $S (= \frac{5}{2})$ in FeCl_3 GIC's is described by

$$H = -2J(\text{Fe-Fe}) \sum_{\langle i,j \rangle} \mathbf{S}_i \cdot \mathbf{S}_j + D(\text{Fe}) \sum_i (S_i^z)^2, \quad (2)$$

where $J(\text{Fe-Fe})$ is the intraplanar exchange interaction and is given by -0.47 K for stage-1 FeCl_3 GIC and by -0.34 K for stage-2 FeCl_3 GIC, respectively, and $D(\text{Fe})$ is the single-ion anisotropy and is given by 0.13 K for stage-1 FeCl_3 GIC and 0.23 K for stage-2 FeCl_3 GIC. The dc magnetic-susceptibility data of FeCl_3 GIC's are given as follows: $\Theta_a = -8.2 \pm 0.8$ K, $\Theta_c = -11.4 \pm 1.8$

K, $P_{\text{eff}}^a = 5.98 \pm 0.05 \mu_B$, $P_{\text{eff}}^c = 5.87 \pm 0.07 \mu_B$ for stage-1 FeCl_3 GIC, and $\Theta_a = -6.0 \pm 1.0$ K, $\Theta_c = -9.0 \pm 2.0$ K, $P_{\text{eff}}^a = 5.97 \pm 0.07 \mu_B$, $P_{\text{eff}}^c = 5.87 \pm 0.07 \mu_B$ for stage-2 FeCl_3 GIC. The FeCl_3 GIC undergoes a magnetic phase transition at the Néel temperature $T_N: T_N = 3.9 \pm 0.3$ K for stage-1 FeCl_3 GIC and $T_N = 3.6 \pm 0.3$ K for stage-2 FeCl_3 GIC.

III. EXPERIMENT

Samples of $\text{Co}_c\text{Mn}_{1-c}\text{Cl}_2\text{-FeCl}_3$ GBIC's were prepared by a sequential intercalation method:¹ the intercalant FeCl_3 was intercalated into the empty graphite galleries of stage-2 $\text{Co}_c\text{Mn}_{1-c}\text{Cl}_2$ GIC. A mixture of well-defined stage-2 $\text{Co}_c\text{Mn}_{1-c}\text{Cl}_2$ GIC based on single-crystal kish graphite and single-crystal FeCl_3 was sealed in vacuum inside Pyrex glass tubing, and was kept at 330 °C for two weeks. The stoichiometry of GBIC samples, represented by $\text{C}_n(\text{Co}_c\text{Mn}_{1-c}\text{Cl}_2)_{1-b}(\text{FeCl}_3)_b$, was determined from a weight-uptake measurement. The Fe concentration of GBIC samples denoted by b_e was also determined by the electron microprobe measurement with the use of a scanning electron microscope (Model Hitachi S-450). The electrons having a kinetic energy of 20 keV penetrate the sample to a depth of the order of 2 μm , spreading out a similar distance. The emitted characteristic x ray was analyzed by means of the energy-dispersion method.

In order to confirm the stacking sequence of GBIC samples the (00L) x-ray-diffraction measurements were made at 300 K by using a Huber double-circle diffractometer with a Siemens 2.0-kW x-ray generator. The highly sensitive measurements of magnetization were carried out with a superconducting quantum interference device (SQUID) magnetometer (Model VTS-905 SQUID system, manufactured by S.H.E. Corporation). The low-field SQUID magnetization measurements were performed in the following steps: (i) A sample having a weight of 4–7 mg was first cooled to 2 K from 300 K in 5 min in the absence of external magnetic field. A field of 1 Oe was then applied along any direction perpendicular to the c axis. (ii) The temperature dependence of zero-field cooled (ZFC) magnetization, M_{ZFC} , was measured while increasing temperature from 2 to 10 K. (iii) The sample was again cooled in the field of 1 Oe and the temperature dependence of field-cooled (FC) magnetization, M_{FC} , was measured while decreasing temperature from 10 to 2 K. The ac magnetic susceptibility was measured by an ac Hartshorn bridge method in the temperature range between 2.8 and 14 K. An ac magnetic field with frequency $\nu = 330$ Hz and amplitude $h = 300$ mOe was applied along any direction in the c plane of the GBIC sample. The dc magnetic susceptibility of these samples was measured by the Faraday balance method in the temperature range between 1.5 and 300 K. A magnetic field of $100 \leq H \leq 2$ kOe was applied in any direction in the c plane of GBIC samples.

IV. RESULTS

A. Sample characterization

We have measured the (00L) x-ray-diffraction pattern for $\text{Co}_c\text{Mn}_{1-c}\text{Cl}_2\text{-FeCl}_3$ GBIC's having the stacking se-

quence of $G\text{-Co}_c\text{Mn}_{1-c}\text{Cl}_2\text{-G-FeCl}_3\text{-G}\dots$. A typical example of an x-ray-diffraction pattern is shown in Fig. 1(a) for $\text{Co}_{0.25}\text{Mn}_{0.75}\text{Cl}_2\text{-FeCl}_3$ GBIC as a function of the scattering wave vector Q_c . Sharp Bragg peaks appear around $|Q_c| = (2\pi/d)L$ for even integer L with $d = 18.87 \pm 0.12$ Å. Since the distance of $G\text{-Co}_c\text{Mn}_{1-c}\text{Cl}_2\text{-G}$ layers is similar to that of $G\text{-FeCl}_3\text{-G}$ layers, and the atomic form factor of $\text{Co}_c\text{Mn}_{1-c}$ is almost the same as that of Fe, the scattering intensity for odd integer L is very weak. The c -axis repeat distance d is increased from 12.871 Å for stage-2 $\text{Co}_{0.25}\text{Mn}_{0.75}\text{Cl}_2$ GIC to 18.87 Å after the sequential intercalation of FeCl_3 . The absence of Bragg peaks from stage-2 $\text{Co}_{0.25}\text{Mn}_{0.75}\text{Cl}_2$ GIC indicates that the empty graphite galleries are completely filled with FeCl_3 layers on sequential intercalation. The c -axis repeat distance d of $\text{Co}_c\text{Mn}_{1-c}\text{Cl}_2\text{-FeCl}_3$

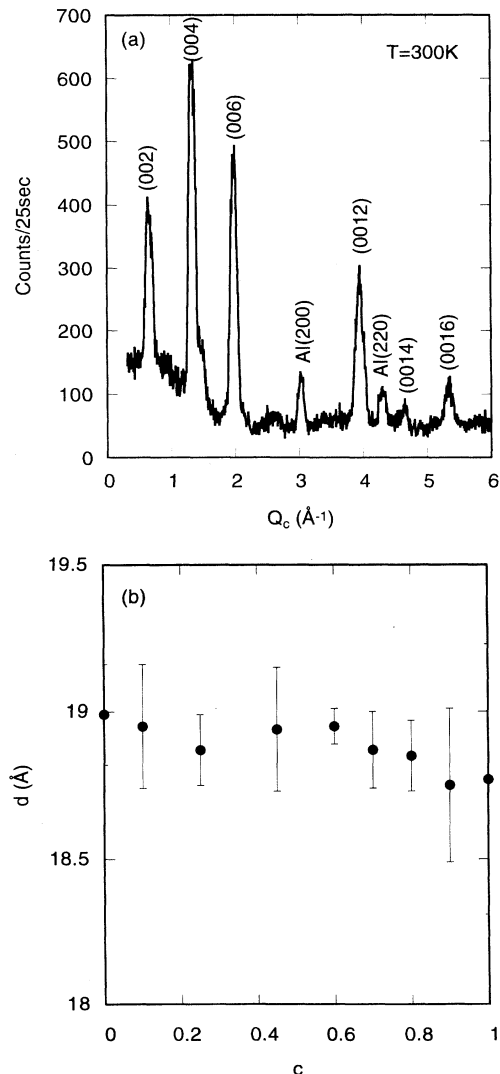


FIG. 1. (a) (00L) x-ray-diffraction pattern of $\text{Co}_c\text{Mn}_{1-c}\text{Cl}_2\text{-FeCl}_3$ GBIC with $c = 0.25$ at 300 K. $Q_c = L(2\pi/d)$ with $d = 18.87 \pm 0.12$ Å. (b) The c -axis repeat distance d vs concentration c for $\text{Co}_c\text{Mn}_{1-c}\text{Cl}_2\text{-FeCl}_3$ GBIC's.

GBIC samples is determined from their (00L) x-ray diffraction and is listed in Table I. The data of d vs concentration c for $\text{Co}_c\text{Mn}_{1-c}\text{Cl}_2\text{-FeCl}_3$ GBIC's is also plotted in Fig. 1(b). The c -axis repeat distance seems to vary linearly with concentration c in spite of large uncertainty in d because of the c -axis stacking disorder of the GBIC samples.

The ideal stoichiometry of $\text{CoCl}_2\text{-FeCl}_3$ GBIC and $\text{MnCl}_2\text{-FeCl}_3$ GBIC is estimated as $\text{C}_n(\text{CoCl}_2)_{1-b}(\text{FeCl}_3)_b$ with $n=4.99$ and $b=0.40$, and $\text{C}_n(\text{MnCl}_2)_{1-b}(\text{FeCl}_3)_b$ with $n=5.18$ and $b=0.42$. The ideal value of b for $\text{Co}_c\text{Mn}_{1-c}\text{Cl}_2\text{-FeCl}_3$ GBIC's is expected to be between 0.40 and 0.42. The stoichiometry of $\text{Co}_c\text{Mn}_{1-c}\text{Cl}_2\text{-FeCl}_3$ GBIC samples determined from the weight-uptake measurements is listed in Table I. The Fe concentration b in $\text{Co}_c\text{Mn}_{1-c}\text{Cl}_2\text{-FeCl}_3$ GBIC's is between 0.32 and 0.47 except for $c=0.15$ and 0.80 samples. These values of b are close to the ideal value. We have also determined the stoichiometry of these GBIC's by electron microprobe measurements. The value of Fe concentration defined as b_e are also listed in Table I. The Fe concentration b_e of $\text{Co}_c\text{Mn}_{1-c}\text{Cl}_2\text{-FeCl}_3$ GBIC's is relatively larger than that determined from the weight-uptake measurements. The electron microprobe measurement determines the average Fe concentration over the depth of several μm from the sample surface where bulk intercalant FeCl_3 may still remain.

B. Magnetic phase transitions

1. SQUID magnetization

We have measured the low-field SQUID magnetization of $\text{Co}_c\text{Mn}_{1-c}\text{Cl}_2\text{-FeCl}_3$ GBIC's below 10 K. Figure 2 shows the temperature dependence of the FC magnetization (M_{FC}), and ZFC magnetization (M_{ZFC}), and the difference δ ($=M_{\text{FC}}-M_{\text{ZFC}}$) for $\text{Co}_c\text{Mn}_{1-c}\text{Cl}_2\text{-FeCl}_3$ GBIC's with (a) $c=1$, (b) 0.9, (c) 0.7, (d) 0.55, (e) 0.45, (f) 0.3, and (g) 0, where the data of $c=0$ were taken for the

TABLE I. Stoichiometry of $\text{Co}_c\text{Mn}_{1-c}\text{Cl}_2\text{-FeCl}_3$ GBIC samples: $\text{C}_n(\text{Co}_c\text{Mn}_{1-c}\text{Cl}_2)_{1-b}(\text{FeCl}_3)_b$, where b and b_e are the Fe concentrations determined from weight-uptake measurements and electron microprobe measurements, respectively, and d is the c -axis repeat distance.

Sample No.	c	n	b	b_e	d (Å)
1	0	7.95	0.34	0.53	18.99 ± 0.17
2	0	7.68	0.38		
3	0.05	8.63	0.43		
4	0.1	8.08	0.47		18.95 ± 0.21
5	0.15	7.38	0.56		
6	0.2	11.1	0.32		
7	0.25	5.87	0.45		18.87 ± 0.12
8	0.45	6.14	0.45	0.86	18.94 ± 0.21
9	0.6	5.50	0.36	0.67	18.95 ± 0.06
10	0.7	6.92	0.35	0.72	18.87 ± 0.13
11	0.8	7.98	0.26		18.85 ± 0.12
12	0.9	9.48	0.38	0.70	18.75 ± 0.26
13	1	6.40	0.37	0.29	18.77 ± 0.46

sample No. 1 listed in Table I. The difference δ is a measure of the irreversible effect of magnetization. Here we define the characteristic temperature T_0 as a temperature above which δ becomes zero. This value of T_0 will be compared with that of the critical temperature T_c which will be determined from the ac magnetic susceptibility in Sec. IV B 2. For $c=1$ [Fig. 2(a)], M_{FC} drastically increases as temperature decreases below T_0 (≈ 9.1 K), and reaches a value of 700 emu/av mol at 2.5 K, while M_{ZFC} deviates downward from M_{FC} below T_0 and shows a broad peak at T_{max} (≈ 7.5 K). The difference δ appearing below T_0 monotonically increases with the decrease of temperature. For $c=0.9$ [Fig. 2(b)], M_{ZFC} shows a cusplike form around T_{max} (≈ 7 K). The difference δ appearing below T_0 (≈ 9 K) shows a broad peak around 5 K. For $c=0.7$ [Fig. 2(c)], M_{ZFC} tends to increase in two steps as temperature decreases. The difference δ increases with decreasing temperature below T_0 (≈ 9 K), and becomes constant below 5 K. For $c=0.55$ and 0.45 [Figs. 2(d) and (e)], the irreversible effect still appears below T_0 (≈ 9 K), but no broad peak is observed in M_{ZFC} . The value of δ at 2.5 K is much smaller than that for $c=1$. For $c=0.3$ [Fig. 2(f)], the temperature dependence of M_{FC} almost coincides with that of M_{ZFC} above 4 K, indicating no irreversible effect of magnetization. For $c=0$ [Fig. 2(g)], M_{ZFC} shows a cusp-like form around 4 K, and slightly deviates downward from M_{FC} below T_0 (≈ 9 K), slightly showing an irreversible effect of magnetization. The value of M_{FC} at 2.5 K for $c=0$ is relatively larger than that for $c=0.3$. These two results show some evidence for the ferromagnetic behavior in $\text{MnCl}_2\text{-FeCl}_3$ GBIC at low temperatures. The origin of this ferromagnetic behavior will be discussed in Sec. V B.

Thus our data of low-field SQUID magnetization for $\text{Co}_c\text{Mn}_{1-c}\text{Cl}_2\text{-FeCl}_3$ GBIC's shows the irreversible effect of magnetization below T_0 over the entire concentration c except for $c=0.3$. The characteristic temperature T_0 seems to be independent of concentration c ($T_0 \approx 9$ K). On the other hand the SQUID magnetization of stage-2 $\text{Co}_c\text{Mn}_{1-c}\text{Cl}_2$ GIC's (Ref. 12) shows the irreversible effect of magnetization for $0.8 \leq c \leq 1$ below T_c : T_c decreases with decreasing concentration c . The magnetic properties of $\text{Co}_c\text{Mn}_{1-c}\text{Cl}_2\text{-FeCl}_3$ GBIC's with $0.8 \leq c < 1$ is found to be quite different from those of stage-2 $\text{Co}_c\text{Mn}_{1-c}\text{Cl}_2$ GIC's with same concentration range. The spin-ordering process in $\text{Co}_c\text{Mn}_{1-c}\text{Cl}_2\text{-FeCl}_3$ GBIC's is considered to be much more complicated than that in stage-2 $\text{Co}_c\text{Mn}_{1-c}\text{Cl}_2$ GIC's because of the interplanar interactions between $\text{Co}_c\text{Mn}_{1-c}\text{Cl}_2$ layers and FeCl_3 layers. The difference in the spin-ordering process of $\text{Co}_c\text{Mn}_{1-c}\text{Cl}_2\text{-FeCl}_3$ GBIC's and stage-2 $\text{Co}_c\text{Mn}_{1-c}\text{Cl}_2$ GIC's will be discussed in detail in Sec. V.

2. ac magnetic susceptibility

In order to determine the critical temperature T_c , we have measured the real part of ac magnetic susceptibility χ' for $\text{Co}_c\text{Mn}_{1-c}\text{Cl}_2\text{-FeCl}_3$ GBIC's with $0 \leq c \leq 1$ in the temperature range between 2.8 and 14 K. Figure 3(a) shows the temperature dependence of χ' for

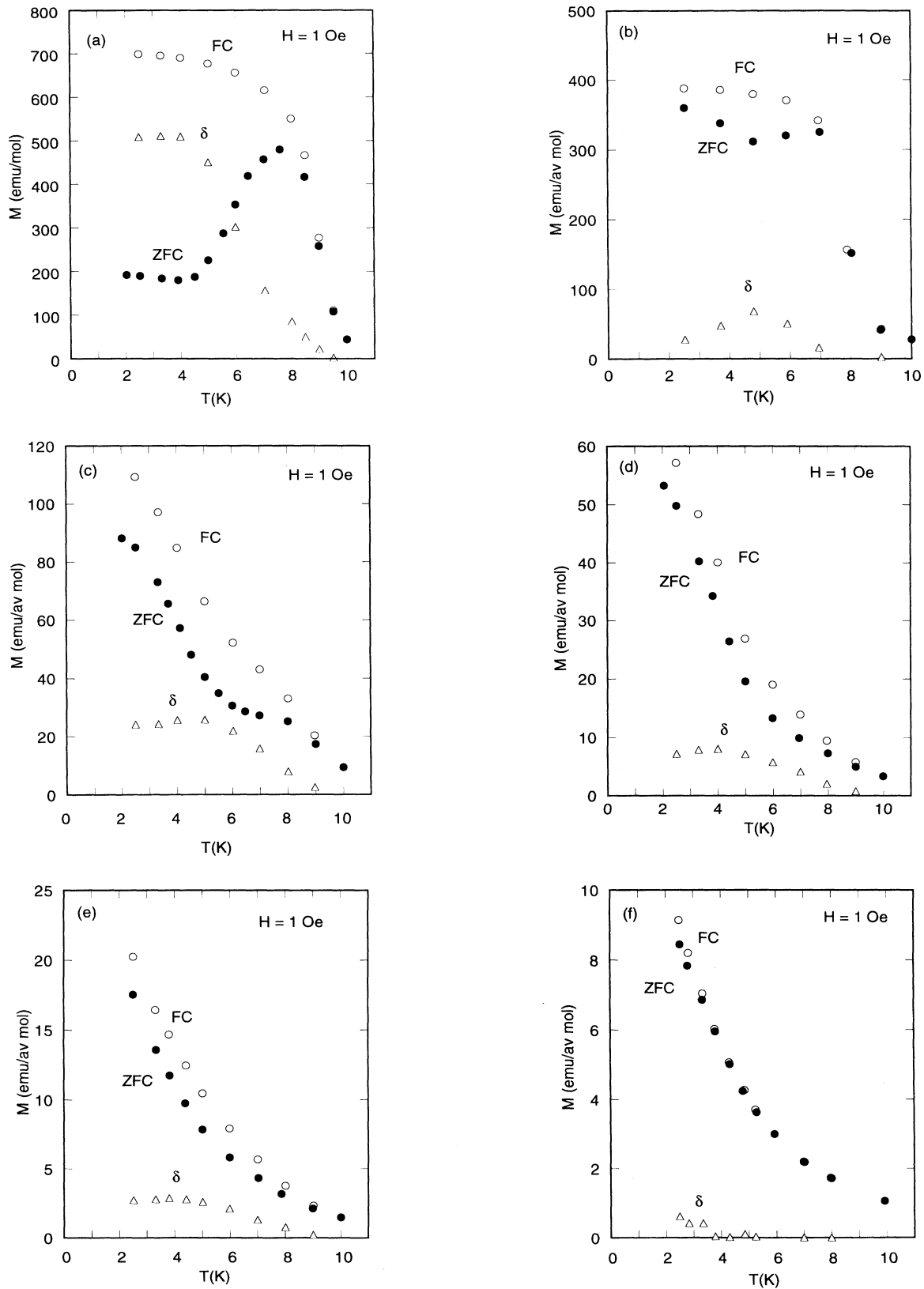


FIG. 2. Temperature variation of field-cooled magnetization M_{FC} (\circ), zero-field-cooled magnetization M_{ZFC} (\bullet), and $\delta (= M_{\text{FC}} - M_{\text{ZFC}})$ (\triangle) for $\text{Co}_2\text{Mn}_{1-c}\text{Cl}_2\text{-FeCl}_3$ GBIC's with (a) $c = 1$ (Ref. 9), (b) 0.9, (c) 0.7, (d) 0.55, (e) 0.45, (f) 0.3, and (g) 0 (sample No. 1), where $H = 1$ Oe and $H \perp c$.

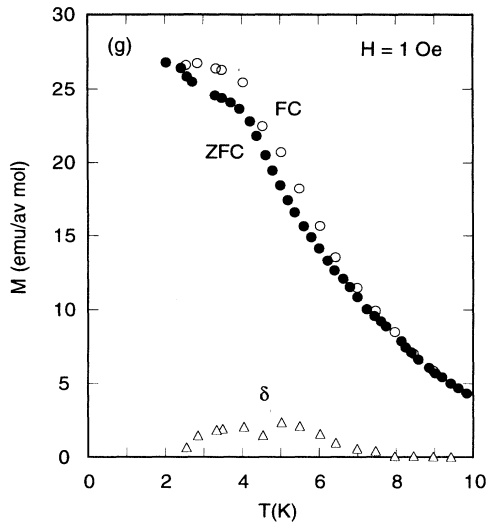


FIG. 2 (Continued).

$\text{Co}_c\text{Mn}_{1-c}\text{Cl}_2\text{-FeCl}_3$ GBIC's with $c = 1, 0.9, 0.8, 0.7$. The susceptibility χ' for each concentration c shows a broad peak at a temperature which is defined as the critical temperature T_c . This result implies that the spins in the $\text{Co}_c\text{Mn}_{1-c}\text{Cl}_2$ layers are ferromagnetically ordered below T_c . The peak of χ' drastically decreases as the concentration c decreases from $c = 1$ to $c = 0.7$. The critical temperature T_c shifts to the lower temperature side as the concentration c decreases. The concentration dependence of T_c for $\text{Co}_c\text{Mn}_{1-c}\text{Cl}_2\text{-FeCl}_3$ GBIC's is in contrast to that of the characteristic temperature T_0 (Sec. IV B 1): T_0 seems to be independent of the concentration c . Note that no peak in χ' is observed for $c = 0.45, 0.25, 0.2, 0.15, 0.1$, and 0.05 above 2.8 K, indicating no ferromagnetic phase transition for these concentrations.

We have also measured the ac magnetic susceptibility of $\text{MnCl}_2\text{-FeCl}_3$ GBIC for two samples (samples No. 1 and 2). Figure 3(b) shows the temperature dependence of χ' for $\text{MnCl}_2\text{-FeCl}_3$ GBIC (sample No. 1). This ac susceptibility χ' clearly shows a broad peak at $T_c = 6.9$ K, although the peak value of χ' is relatively smaller than that for $c = 0.7$. Here it should be noted that the peak temperature of χ' for $c = 0$ is dependent on samples. We find that χ' for the sample No. 2 shows a broad peak at $T_c = 5.9$ K which is a little lower than that of sample No. 1. The broad peak in χ' for $c = 0$ suggests that the nature of the magnetic phase transition at T_c is ferromagnetic. The ferromagnetic behavior is consistent with the irreversible effect of magnetization observed in the SQUID magnetization of $c = 0$ sample (Sec. IV B 1).

Figure 4 shows the concentration c dependence of T_c for $\text{Co}_c\text{Mn}_{1-c}\text{Cl}_2\text{-FeCl}_3$ GBIC's (closed circles) and stage-2 $\text{Co}_c\text{Mn}_{1-c}\text{Cl}_2$ GIC's (open circles): $T_c = 9.1$ K for $c = 1$, 7.82 K for $c = 0.9$, 5.58 K for $c = 0.8$, $T_c = 3.7$ K for $c = 0.7$, and $T_c = 5.9$ K or 6.9 K for $c = 0$ for $\text{Co}_c\text{Mn}_{1-c}\text{Cl}_2\text{-FeCl}_3$ GBIC's, and $T_c = 8.20$ K for $c = 1$, 7.68 K for $c = 0.9$, 6.18 K for $c = 0.85$, 6.62 K for $c = 0.8$, 3.80 K for $c = 0.7$, and 4.16 K for $c = 0.6$ for stage-2 $\text{Co}_c\text{Mn}_{1-c}\text{Cl}_2$ GIC's (Ref. 11). It is found from

Fig. 4 that the value of T_c for $\text{Co}_c\text{Mn}_{1-c}\text{Cl}_2\text{-FeCl}_3$ GBIC's is almost the same as that for stage-2 $\text{Co}_c\text{Mn}_{1-c}\text{Cl}_2$ GIC's with the same concentration c for $0.7 \leq c < 1$: T_c drastically decreases with decreasing concentration c and tends to be zero around $c = 0.5$ corresponding to the percolation threshold predicted for the 2D systems on the triangular lattice.

3. Low-temperature dc magnetic susceptibility

We have measured the dc magnetic susceptibility for $\text{Co}_c\text{Mn}_{1-c}\text{Cl}_2\text{-FeCl}_3$ GBIC's with $0 \leq c \leq 1$ in the temperature range between 1.5 and 30 K. The magnetic field of 100 Oe was applied along any direction perpendicular to

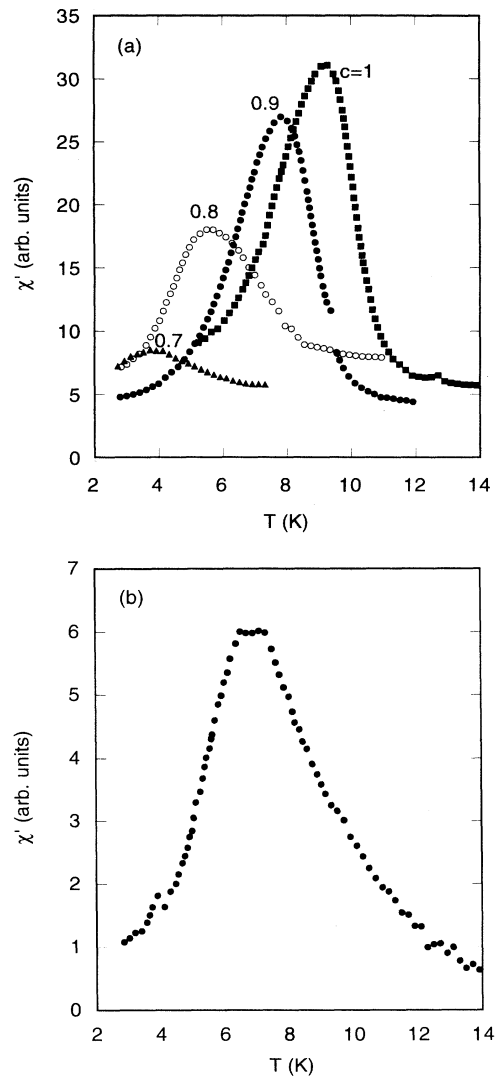


FIG. 3. (a) Temperature dependence of real part of ac magnetic susceptibility χ' for $\text{Co}_c\text{Mn}_{1-c}\text{Cl}_2\text{-FeCl}_3$ GBIC's with $c = 1$ (■), 0.9 (●), 0.8 (○), and 0.7 (▲). (b) Temperature dependence of real part of ac magnetic susceptibility χ' for $\text{MnCl}_2\text{-FeCl}_3$ GBIC (sample No. 1). The ac magnetic field of $\nu = 330$ Hz and $h = 300$ mOe is applied along any direction perpendicular to the c axis.

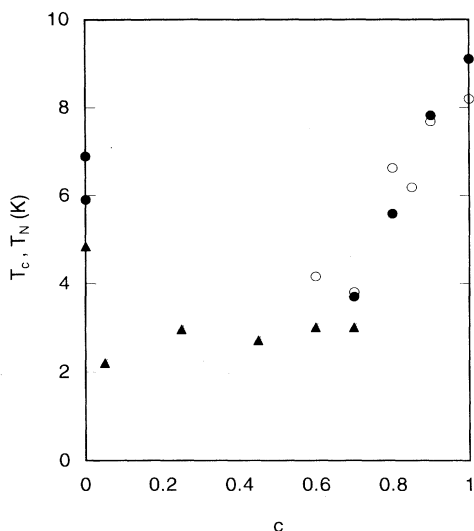


FIG. 4. Critical temperature T_c vs concentration c for $\text{Co}_c\text{Mn}_{1-c}\text{Cl}_2\text{-FeCl}_3$ GBIC's (●) and stage-2 $\text{Co}_c\text{Mn}_{1-c}\text{Cl}_2$ GIC's (○) (Ref. 10) determined from ac magnetic-susceptibility measurements. The closed triangles (▲) denote the Néel temperature T_N of $\text{Co}_c\text{Mn}_{1-c}\text{Cl}_2\text{-FeCl}_3$ GBIC's with $0 \leq c \leq 0.7$ determined from dc magnetic susceptibility.

the c axis. Figure 5(a) shows the temperature dependence of M/H for $\text{Co}_c\text{Mn}_{1-c}\text{Cl}_2\text{-FeCl}_3$ GBIC's with $c = 1, 0.9, 0.8, 0.7, 0.6, 0.45,$ and 0.25 . For $c = 1$, the susceptibility M/H drastically increases with decreasing temperature around T_c ($=9.1$ K), exhibits a plateau-like form between 7 and 4 K, and then slightly decreases below ≈ 4 K. For $c = 0.9$, the susceptibility M/H gradually increases with decreasing temperature around T_c ($=7.82$ K), shows a broad peak around 4.4 K, and then slightly decreases below ≈ 4 K. For $c = 0.8$, the susceptibility M/H has a plateau-like form around 4 K. The decrease of M/H with decreasing temperature is also observed below 3 K. The maximum susceptibility decreases as the concentration c decreases for $0.25 \leq c \leq 1$.

Figure 5(b) shows the temperature dependence of M/H for $\text{Co}_c\text{Mn}_{1-c}\text{Cl}_2\text{-FeCl}_3$ GBIC's with $c = 0.25, 0.15, 0.05,$ and 0 (sample No. 1). For $c = 0$, the susceptibility M/H shows a broad peak around 4.5 K. This peak temperature is appreciably higher than that for $c = 0.25$ and 0.05 . The maximum susceptibility for $c = 0$ is about 11 emu/mol and is much larger than that for $c = 0.05$ and 0.25 , indicating the ferromagnetic behavior of this system. This result is consistent with that derived from the SQUID magnetization (Sec. IV B 1) and ac magnetic susceptibility (Sec. IV B 2). Although the data of M/H vs T for $c = 0.2$ and 0.1 are not shown in Fig. 5(b), the values of M/H for $c = 0.2$ and 0.1 almost coincide with that for $c = 0.15$ at the same temperature for $1.5 \leq T \leq 10$ K. The monotonic increase of M/H for $c = 0.2, 0.15,$ and 0.1 with the decrease of temperature shows that these compounds undergo no magnetic phase transition at least above 1.5 K. We find that the dc magnetic susceptibility of $\text{Co}_c\text{Mn}_{1-c}\text{Cl}_2\text{-FeCl}_3$ GBIC's with $c = 0, 0.05, 0.25, 0.45, 0.6,$ and 0.7 shows a broad peak around 3–4 K.

The peak temperatures are denoted as closed triangles in Fig. 4.

For comparison, the temperature dependence of susceptibility M/H for stage-2 $\text{Co}_c\text{Mn}_{1-c}\text{Cl}_2$ GIC's ($1.5 \leq T \leq 12$ K) is shown in Fig. 6(a). From this figure we can see the following results: (i) No appreciable peak of M is observed over the entire concentration for $1.5 \leq T \leq 4$ K, although the data of M/H vs T for $0 \leq c < 0.45$ are not shown in Fig. 6(a). (ii) The value of M/H at 2 K for stage-2 $\text{Co}_c\text{Mn}_{1-c}\text{Cl}_2$ GIC's is much larger than that for $\text{Co}_c\text{Mn}_{1-c}\text{Cl}_2\text{-FeCl}_3$ GBIC's with the same concentration c . (iii) The GIC's with $c \geq 0.45$ undergo ferromagnetic phase transitions at T_c . These features of stage-2 $\text{Co}_c\text{Mn}_{1-c}\text{Cl}_2$ GIC's are in contrast to

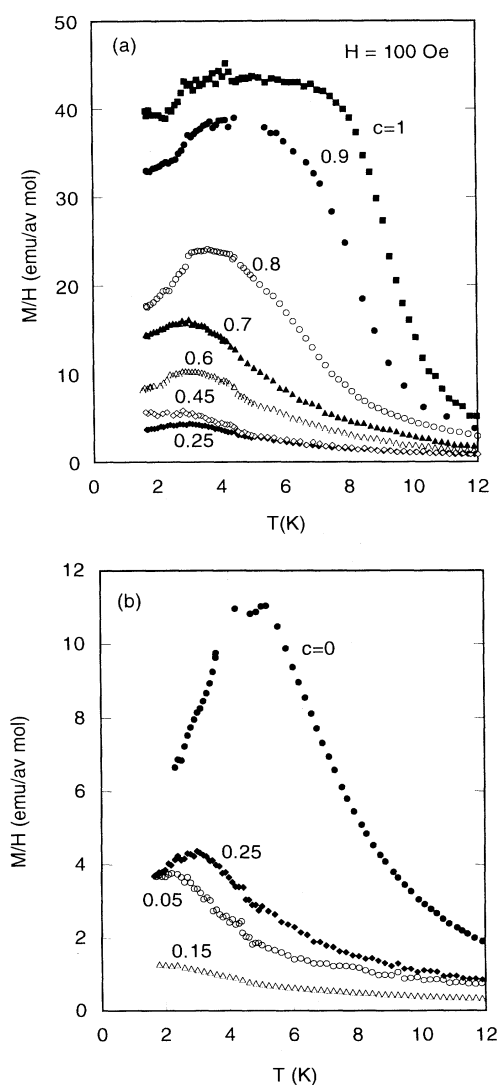


FIG. 5. Temperature dependence of dc magnetic susceptibility ($=M/H$) for $\text{Co}_c\text{Mn}_{1-c}\text{Cl}_2\text{-FeCl}_3$ GBIC's, where $H = 100$ Oe and $H \perp c$. (a) $c = 1$ (■), 0.9 (●), 0.8 (○), 0.7 (▲), 0.6 (△), 0.45 (◇), and 0.25 (◆). (b) $c = 0.25$ (◆), 0.15 (△), 0.05 (○), and 0 (sample No. 1, ●). Note that the data for $c = 0.15$ were taken at $H = 500$ Oe.

those of $\text{Co}_c\text{Mn}_{1-c}\text{Cl}_2\text{-FeCl}_3$ GBIC's. The broad peak of M/H vs T near 3–4 K is observed for $\text{Co}_c\text{Mn}_{1-c}\text{Cl}_2\text{-FeCl}_3$ GBIC's with $0.25 \leq c \leq 0.7$, but not for stage-2 $\text{Co}_c\text{Mn}_{1-c}\text{Cl}_2$ GIC's. This broad peak may arise as a result of the appearance of long-range spin order in the FeCl_3 layers. If this long-range spin order in the FeCl_3 layers is of the same type as the antiferromagnetic spin order of FeCl_3 GIC,^{21,22} such a broad peak should be observed near 3–4 K in the dc magnetic susceptibility of FeCl_3 GIC's. In order to confirm the validity of this assumption, we have measured the dc magnetic susceptibility of stage-2 FeCl_3 GIC, where a magnetic field of $H = 750$ Oe was applied along any direction perpendicular to the c axis. Figure 6(b) shows the temperature dependence of stage-2 FeCl_3 GIC based on highly oriented pyrolytic graphite in the temperature range between

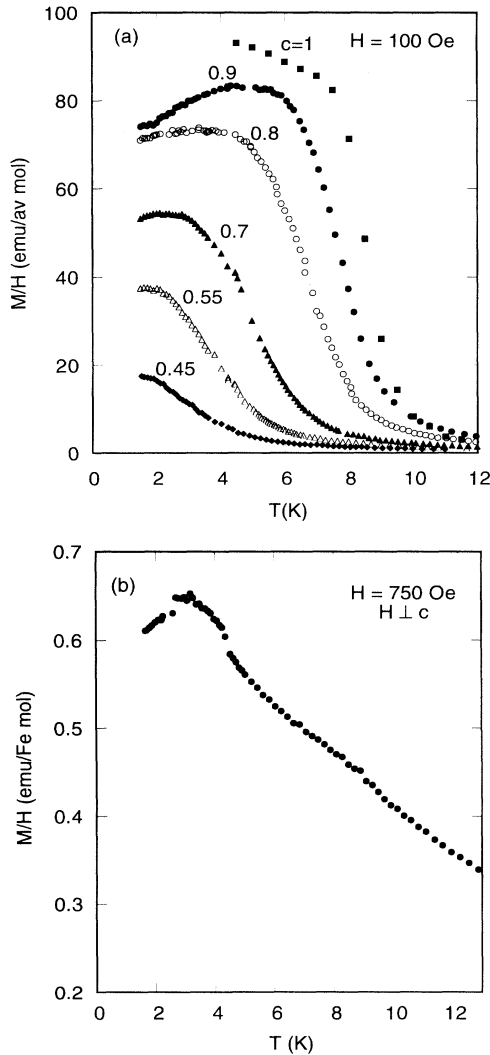


FIG. 6. (a) Temperature dependence of dc magnetic susceptibility for stage-2 $\text{Co}_c\text{Mn}_{1-c}\text{Cl}_2\text{-FeCl}_3$ GIC's. (Ref. 10) $H = 100$ Oe and $\mathbf{H} \perp c$. $c = 1$ (■), 0.9 (●), 0.8 (○), 0.7 (▲), 0.55 (△), and 0.45 (◆). (b) Temperature dependence of dc magnetic susceptibility for stage-2 FeCl_3 GIC. $H = 750$ Oe and $\mathbf{H} \perp c$.

1.5 and 20 K. The susceptibility M/H has a small peak at the Néel temperature T_N ($=3.2$ K) below which the antiferromagnetic phase appears. This Néel temperature is a little lower than that determined by Ohhashi and Tsujikawa^{21,22} from the Mössbauer effect: $T_N = 3.6 \pm 0.3$ K for stage-2 FeCl_3 GIC. Therefore this result implies that the broad peak around 3–4 K observed in $\text{Co}_c\text{Mn}_{1-c}\text{Cl}_2\text{-FeCl}_3$ GBIC's is due to the antiferromagnetic spin order occurring in the FeCl_3 layers.

C. Paramagnetic susceptibility

We have measured the dc magnetic susceptibility of $\text{Co}_c\text{Mn}_{1-c}\text{Cl}_2\text{-FeCl}_3$ GBIC's with $c = 0, 0.05, 0.1, 0.15, 0.2, 0.25, 0.45, 0.6, 0.7, 0.8,$ and 0.9 in the temperature range between 20 and 300 K. A magnetic field of $H = 2$ kOe was applied along any direction perpendicular to the c axis. A least-squares fit of the dc magnetic-susceptibility data for $150 \leq T \leq 300$ K to the Curie-Weiss law

$$\chi_M = \frac{C_M}{T - \Theta} + \chi_M^0, \quad (3)$$

yields the Curie-Weiss constant C_M (emu K/av mol), the Curie-Weiss temperature Θ (K), and the temperature-independent susceptibility χ_M^0 (emu/av mol). The Curie-Weiss constant C_M is related to the effective magnetic moment by $C_M = N_A \mu_B^2 P_{\text{eff}}^2 / 3k_B$. The parameters of Θ , C_M , and P_{eff} for each concentration are listed in Table II. Figure 7 shows the plots of Θ vs c for $\text{Co}_c\text{Mn}_{1-c}\text{Cl}_2\text{-FeCl}_3$ GBIC's (closed circles). The data of Θ vs c for $\text{Co}_c\text{Mn}_{1-c}\text{Cl}_2\text{-FeCl}_3$ GBIC's are in contrast to those for stage-2 $\text{Co}_c\text{Mn}_{1-c}\text{Cl}_2$ GIC's.¹⁰ The value of Θ for $\text{Co}_c\text{Mn}_{1-c}\text{Cl}_2\text{-FeCl}_3$ GBIC's is positive for all concentration except for $c = 0.2$, while the value of Θ for stage-2 $\text{Co}_c\text{Mn}_{1-c}\text{Cl}_2$ GIC's monotonically increases with increasing concentration: Θ is negative for $0 \leq c < 0.2$ and positive for $0.2 < c \leq 1$. It is predicted from the molecular field theory⁹ that Θ of $\text{Co}_c\text{Mn}_{1-c}\text{Cl}_2\text{-FeCl}_3$ GBIC's with the stoichiometry of $C_n(\text{Co}_c\text{Mn}_{1-c}\text{Cl}_2)_{1-b}(\text{FeCl}_3)_b$ is de-

TABLE II. Curie-Weiss temperature Θ , Curie-Weiss constant C_M and average effective magnetic moment P_{eff} for $\text{Co}_c\text{Mn}_{1-c}\text{Cl}_2\text{-FeCl}_3$ GBIC's.

Sample No.	c	Θ (K)	C_M (emu K/av mol)	P_{eff} (μ_B /av atom)
1	0	12.47±0.10	4.52	6.01
2	0	5.88±0.32	4.76	6.17
3	0.05	3.81±0.35	4.90	6.26
4	0.1	9.62±0.33	4.26	5.84
5	0.15	5.05±0.25	4.45	5.97
6	0.2	-1.26±0.37	4.70	6.13
7	0.25	9.12±0.53	4.16	5.77
8	0.45	6.16±0.42	3.85	5.55
9	0.6	3.05±0.34	4.27	5.85
10	0.7	9.97±0.45	4.51	6.00
11	0.8	10.38±0.47	4.68	6.12
12	0.9	19.69±0.44	3.99	5.65
13	1	21.99±0.15	3.78	5.50

scribed by

$$\Theta(c; \text{GBIC}) = \frac{(1-b)P_{\text{eff}}^2(c; \text{RMGIC})\Theta(c; \text{RMGIC}) + bP_{\text{eff}}^2(\text{Fe}^{3+})\Theta(\text{Fe}^{3+})}{P_{\text{eff}}^2(c; \text{GBIC})}, \quad (4)$$

where $P_{\text{eff}}(c; \text{RMGIC})$ and $\Theta(c; \text{RMGIC})$ are the effective magnetic moment and the Curie-Weiss temperature of stage-2 $\text{Co}_c\text{Mn}_{1-c}\text{Cl}_2$ GIC,¹⁰ respectively, $P_{\text{eff}}(c; \text{GBIC})$ is the effective magnetic moment of $\text{Co}_c\text{Mn}_{1-c}\text{Cl}_2\text{-FeCl}_3$ GBIC's, and $P_{\text{eff}}(\text{Fe}^{3+})$ and $\Theta(\text{Fe}^{3+})$ are the effective magnetic moment and the Curie-Weiss temperature of stage-2 FeCl_3 GIC, respectively: $P_{\text{eff}}(\text{Fe}^{3+}) = 6.57\mu_B$ and $\Theta(\text{Fe}^{3+}) = -4.3 \pm 0.2$ K.⁹ In Fig. 7 the open circles denote the values of $\Theta(c; \text{GBIC})$ for $\text{Co}_c\text{Mn}_{1-c}\text{Cl}_2\text{-FeCl}_3$ GBIC's calculated from Eq. (4) with $b = 0.4$. Our data of Θ for $\text{Co}_c\text{Mn}_{1-c}\text{Cl}_2\text{-FeCl}_3$ GBIC's agree well with $\Theta(c; \text{GBIC})$ for $0.4 \leq c \leq 0.8$, but greatly deviate from it for $0 \leq c < 0.2$. The sign of Θ for $\text{Co}_c\text{Mn}_{1-c}\text{Cl}_2\text{-FeCl}_3$ GBIC's is positive for $0 \leq c < 0.2$, while the sign of Θ is predicted to be negative from Eq. (4) with $b = 0.4$. The positive sign of Θ for $0 \leq c < 0.2$ indicates that $\text{Co}_c\text{Mn}_{1-c}\text{Cl}_2\text{-FeCl}_3$ GBIC's magnetically behave like a ferromagnetic system, which is consistent with the results of SQUID magnetization, ac magnetic susceptibility, and dc magnetic susceptibility at low temperatures. Here we note that the data of Θ for stage-2 $\text{Co}_c\text{Mn}_{1-c}\text{Cl}_2$ GIC's fit well with the predicted values of Θ with $b = 0$ over the entire concentration of c .⁹ The ferromagnetic nature of $\text{Co}_c\text{Mn}_{1-c}\text{Cl}_2\text{-FeCl}_3$ GBIC's near $c = 0$ will be discussed in Sec. V B.

Figure 8 shows the plots of P_{eff} vs c for $\text{Co}_c\text{Mn}_{1-c}\text{Cl}_2\text{-FeCl}_3$

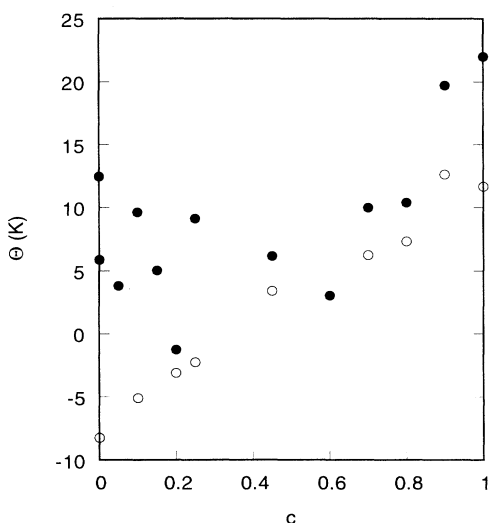


FIG. 7. Curie-Weiss temperature vs concentration c for $\text{Co}_c\text{Mn}_{1-c}\text{Cl}_2\text{-FeCl}_3$ GBIC's (●). The open circles denote the values of Θ for GBIC's predicted from Eq. (4) with $b = 0.4$, where the values of Θ and P_{eff} for stage-2 $\text{Co}_c\text{Mn}_{1-c}\text{Cl}_2$ GIC's (Ref. 10) are used as $\Theta(c; \text{RMGIC})$ and $P_{\text{eff}}(c; \text{RMGIC})$, respectively, and the values of P_{eff} for $\text{Co}_c\text{Mn}_{1-c}\text{Cl}_2\text{-FeCl}_3$ GBIC's are used as $P_{\text{eff}}(c; \text{GBIC})$. $P_{\text{eff}}(\text{Fe}^{3+}) = 6.57\mu_B$ and $\Theta(\text{Fe}^{3+}) = -4.3$ K for stage-2 FeCl_3 GIC.

FeCl_3 GBIC's (closed circles). The concentration dependence of P_{eff} for $\text{Co}_c\text{Mn}_{1-c}\text{Cl}_2\text{-FeCl}_3$ GBIC's seems to be similar to that for stage-2 $\text{Co}_c\text{Mn}_{1-c}\text{Cl}_2$ GIC's:¹⁰ they show a broad peak around $0.7 \leq c \leq 0.9$ and a minimum around $0.25 \leq c \leq 0.45$. It is predicted from the molecular field theory that P_{eff} of $\text{Co}_c\text{Mn}_{1-c}\text{Cl}_2\text{-FeCl}_3$ GBIC's is described by⁹

$$P_{\text{eff}}(c; \text{GBIC}) = [(1-b)P_{\text{eff}}^2(c; \text{RMGIC}) + bP_{\text{eff}}^2(\text{Fe}^{3+})]^{1/2}. \quad (5)$$

In Fig. 8 the open circles denote the values of $P_{\text{eff}}(c; \text{GBIC})$ for $\text{Co}_c\text{Mn}_{1-c}\text{Cl}_2\text{-FeCl}_3$ GBIC's calculated from Eq. (5) with $b = 0.4$, where the data of P_{eff} vs c for stage-2 $\text{Co}_c\text{Mn}_{1-c}\text{Cl}_2$ GIC's are used as $P_{\text{eff}}(c; \text{RMGIC})$. Our data of P_{eff} vs c for $\text{Co}_c\text{Mn}_{1-c}\text{Cl}_2\text{-FeCl}_3$ GBIC's are in good agreement with the open circles for $0 \leq c \leq 0.3$ and $0.6 \leq c \leq 0.8$. Here we note that the P_{eff} of stage-2 $\text{Co}_c\text{Mn}_{1-c}\text{Cl}_2$ GIC's is lower than the theoretical prediction.¹⁰ Such a deviation of P_{eff} may be partly due to a partial replacement of Mn^{2+} ions by Mn^{3+} or Mn^+ ions.¹⁰

V. DISCUSSION

For $\text{Co}_c\text{Mn}_{1-c}\text{Cl}_2\text{-FeCl}_3$ GBIC's the resultant magnetic moment associated with the ferromagnetic spin order

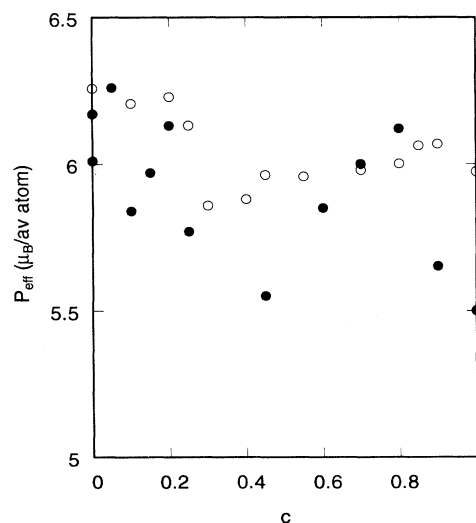


FIG. 8. Effective magnetic moment vs concentration c for $\text{Co}_c\text{Mn}_{1-c}\text{Cl}_2\text{-FeCl}_3$ GBIC's (●). The open circles denote the values of P_{eff} for GBIC's predicted from Eq. (5) with $b = 0.4$, where the values of P_{eff} for stage-2 $\text{Co}_c\text{Mn}_{1-c}\text{Cl}_2$ GIC's are used as $P_{\text{eff}}(c; \text{RMGIC})$. $P_{\text{eff}}(\text{Fe}^{3+}) = 6.57\mu_B$ for stage-2 FeCl_3 GIC's (Ref. 9).

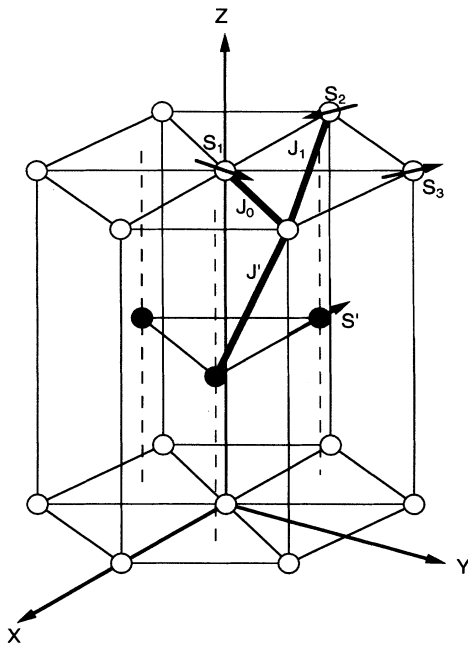


FIG. 9. The hcp-type structure model for $\text{MnCl}_2\text{-FeCl}_3$ GBIC. Open circles denote Mn^{2+} spins on the MnCl_2 layer and closed circles denote Fe^{3+} spins on the FeCl_3 layer. The MnCl_2 layer and FeCl_3 layer are assumed to form a triangular lattice with the same lattice constant.

in the $\text{Co}_c\text{Mn}_{1-c}\text{Cl}_2$ layers drastically decreases with decreasing concentration c . The magnetic phase diagram of T_c vs c for $\text{Co}_c\text{Mn}_{1-c}\text{Cl}_2\text{-FeCl}_3$ GBIC's are complicated due to the spin frustration effect occurring in the $\text{Co}_c\text{Mn}_{1-c}\text{Cl}_2$ layers. It consists of a ferromagnetic cluster glass phase ($0.7 < c < 1$), a coexistence phase with antiferromagnetic phase and spin-glass-like phase ($0.45 \leq c \leq 0.7$), an antiferromagnetic phase ($0.25 \leq c < 0.45$), and ferromagnetic phase ($0 \leq c \leq 0.1$). No magnetic phase transition occurs for $0.1 < c < 0.25$. We discuss the spin-ordering mechanism of each ordered phase in detail.

A. Coexistence of spin-glass phase and antiferromagnetic phase for $0.45 \leq c \leq 0.7$

The dc magnetic susceptibility of $\text{Co}_c\text{Mn}_{1-c}\text{Cl}_2\text{-FeCl}_3$ GBIC's with $0.45 \leq c \leq 0.7$ exhibits a broad peak around $T_N = 3-4$ K, indicating that an antiferromagnetic phase transition occurs in the FeCl_3 layers at T_N . The SQUID magnetization of $\text{Co}_c\text{Mn}_{1-c}\text{Cl}_2\text{-FeCl}_3$ GBIC's with $c = 0.7, 0.55$, and 0.45 shows the irreversible effect of magnetization and has no broad peak in M_{ZFC} , indicating that a spin-glass-like phase occurs in the $\text{Co}_c\text{Mn}_{1-c}\text{Cl}_2$ layers below T_0 . The coexistence of antiferromagnetic phase and spin-glass-like phase is also seen, for example, from the temperature dependence of the ZFC magnetization for $\text{Co}_c\text{Mn}_{1-c}\text{Cl}_2\text{-FeCl}_3$ GBIC with $c = 0.7$: M_{ZFC} drastically changes at T_0 and T_N . These results are in contrast to those of stage-2 $\text{Co}_c\text{Mn}_{1-c}\text{Cl}_2$ GIC's with $0 \leq c \leq 0.7$ showing no irreversible effect of magnetization.

The effective interplanar interaction between $\text{Co}_c\text{Mn}_{1-c}\text{Cl}_2$ layers and FeCl_3 layers becomes strong around T_0 where a 2D short-range spin order drastically grows in the FeCl_3 layers. Although the spin frustration effect arises mainly from the competition between intraplanar ferromagnetic and antiferromagnetic exchange interactions in the $\text{Co}_c\text{Mn}_{1-c}\text{Cl}_2$ layers, this spin frustration effect is considered to be greatly enhanced by the effective interplanar interaction between $\text{Co}_c\text{Mn}_{1-c}\text{Cl}_2$ layers and FeCl_3 layers, leading to the spin-glass-like phase in the $\text{Co}_c\text{Mn}_{1-c}\text{Cl}_2$ layers where spin directions are frozen. A similar type of spin-glass-like phase has been reported for a randomly mixed quasi-2D antiferromagnet and ferromagnet on the square lattice, such as $\text{K}_2\text{Cu}_c\text{Mn}_{1-c}\text{F}_4$,²⁶ $\text{Rb}_2\text{Cr}_c\text{Mn}_{1-c}\text{F}_4$,²⁷ and $\text{K}_2\text{Cu}_c\text{Co}_{1-c}\text{F}_4$ (Ref. 28) with competing nearest-neighbor exchange interactions: a ferromagnetic phase near $c = 1$, antiferromagnetic phase near $c = 0$, and a spin-glass phase in the intermediate concentration.

Here we consider some possibility that the spin-glass-like phase may occur in the FeCl_3 layers. For stage-2 FeCl_3 GIC, Millman and Zimmerman²⁹ have claimed that a sharp peak at 1.7 K observed in the ac magnetic susceptibility is indicative of spin-glass phase behavior. This peak is dramatically enhanced as the number of iron vacancies is increased. Since the number of iron vacancies is inversely proportional to the island radius,³⁰ their results can be interpreted as follows. The growth of the in-plane antiferromagnetic spin correlation length in the FeCl_3 layers is limited by the size of islands, inhibiting an antiferromagnetic long-range spin order. The peak at 1.7 K becomes large as the in-plane spin-correlation length for antiferromagnetic order becomes short. Our spin-glass-like phase observed in $\text{Co}_c\text{Mn}_{1-c}\text{Cl}_2\text{-FeCl}_3$ GBIC's is quite different from that observed by Millman and Zimmerman.²⁹ There is no peak at 1.7 K in the ac susceptibility of $\text{Co}_c\text{Mn}_{1-c}\text{Cl}_2\text{-FeCl}_3$ GBIC's. The irreversible effect of SQUID magnetization for $\text{Co}_c\text{Mn}_{1-c}\text{Cl}_2\text{-FeCl}_3$ GBIC's with $c = 0.55$ [Fig. 2(d)] and 0.45 [Fig. 2(e)] appears below T_0 (≈ 9 K) which is much higher than T_N (≈ 3 K) of the FeCl_3 layer. This difference suggests that the spin-glass-like phase occurs in the $\text{Co}_c\text{Mn}_{1-c}\text{Cl}_2$ layers, not in the FeCl_3 layers for $\text{Co}_c\text{Mn}_{1-c}\text{Cl}_2\text{-FeCl}_3$ GBIC's.

B. Ferromagnetic phase for $0 \leq c \leq 0.1$

There are two models which may explain the ferromagnetic behavior of $\text{Co}_c\text{Mn}_{1-c}\text{Cl}_2\text{-FeCl}_3$ GBIC's with $0 \leq c \leq 0.1$. The first model states that the ferromagnetic behavior occurs in the FeCl_3 layers due to the spin frustration effect arising from (i) the competition between ferromagnetic ($\text{Fe}^{2+}\text{-Fe}^{2+}$) and antiferromagnetic ($\text{Fe}^{3+}\text{-Fe}^{3+}$) intraplanar exchange interactions and (ii) the competition between the Ising and XY spin anisotropies occurring in the FeCl_3 layers due to partial replacement of Fe^{3+} by Fe^{2+} . The second model states that the ferromagnetic behavior occurs in the $\text{Co}_c\text{Mn}_{1-c}\text{Cl}_2$ layers due to the ferromagnetic NN intraplanar exchange interactions J_0 between Mn^{2+} spins which are described in

Sec. II A.

First we consider the first model. Several Mössbauer studies on FeCl₃ GIC's (Refs. 21, 22, and 31–33) give direct evidence for the replacement of a significant amount of Fe³⁺ by Fe²⁺ ions. As described in Sec. II C, the Fe²⁺ spins in FeCl₂ GIC magnetically behave like a quasi-2D Ising ferromagnet on the triangular lattice, while the Fe³⁺ spins in FeCl₃ GIC magnetically behave like a quasi-2D XY antiferromagnet on the honeycomb lattice. We assume that a part of the Fe³⁺ is replaced by Fe²⁺ in the FeCl₃ layers of Co_cMn_{1-c}Cl₂-FeCl₃ GBIC's with 0 ≤ c ≤ 0.1. The magnetic phase transitions of these systems are complicated due to the spin frustration effects arising from competing interactions and competing spin anisotropies.^{26–28} We can predict the magnetic phase diagram of (FeCl₂)_{1-p}(FeCl₃)_p intercalate layers where a strong Ising type anisotropy of Fe²⁺ spins along the c axis compete with a weak XY-type anisotropy of Fe³⁺ spins in the c plane. The ferromagnetic behavior in the Co_cMn_{1-c}Cl₂-FeCl₃ GBIC's with 0 ≤ c ≤ 0.1 can be explained only if a considerable number of Fe³⁺ ions are replaced by Fe²⁺ ions in the inner part of small islands in the FeCl₃ layers. This possible large mole ratio of Fe²⁺ to Fe³⁺ may be related to the charge transfer occurring in the Co_cMn_{1-c}Cl₂ layers. According to Baron *et al.*,³⁴ the charge transfer of ρ = 0.07 electrons per carbon atom occurs from the graphite π band to the periphery of islands for MnCl₂ GIC. This value for the charge transfer is the largest observed for the acceptor-type GIC's: for example, ρ ≈ 0.01 for NiCl₂ GIC and probably for CoCl₂ GIC. Here we can only say that the model is appropriate if the large mole ratio of Fe²⁺ to Fe³⁺ is realized in these systems.

Next we discuss the second model. We consider only the case of MnCl₂-FeCl₃ GBIC. As described in Sec. II A, the in-plane spin structure of stage-2 MnCl₂ GIC is rather complicated due to the frustrated nature of the 2D XY antiferromagnet on the triangular lattice. This incommensurate in-plane spin structure can be realized when the ferromagnetic NN interaction (J_0) competes with the antiferromagnetic NNN (J_1), third NN (J_2), and fourth NN (J_3) interactions: for example, J_0, J_1, J_2 , and J_3 are chosen as 0.38, -0.33, -0.30, and 0.038 K, respectively.²⁰

Sakakibara³⁵ has discussed a possible spin structure of the system with a hexagonal close-packed (hcp)-type structure as shown in Fig. 9, where the sign of J_0, J_1 , and J' are not specified. He shows that (i) the triangular in-plane spin structure is unstable against an infinitesimal interplanar interaction J' , and that (ii) two kinds of incommensurate spin structures appear depending on the sign of J_1 . The incommensurate spin structure arises from a kind of spin frustration effect in the hcp-type structure. In Fig. 9 three spins $\mathbf{S}_1, \mathbf{S}_2$, and \mathbf{S}_3 are located in the same layer and one spin \mathbf{S}' is located on the adjacent layer. The interplanar interaction energy between the spin \mathbf{S}' and a set of spins $\mathbf{S}_1, \mathbf{S}_2$, and \mathbf{S}_3 through J', E , is described by

$$E = -g\mu_B \mathbf{S}' \cdot \mathbf{H}'_E, \quad (6)$$

where \mathbf{H}'_E is the interplanar exchange field which the spin \mathbf{S}' experiences and is given by

$$\mathbf{H}'_E = 2J'(\mathbf{S}_1 + \mathbf{S}_2 + \mathbf{S}_3)/g\mu_B. \quad (7)$$

For the $\sqrt{3} \times \sqrt{3}$ spin structure with spins on three sublattices forming an angle of 120° with respect to each other, there is no change in E with J' because $|\mathbf{H}'_E| = 0$. For an incommensurate spin structure, $|\mathbf{H}'_E|$ does not reduce to zero. The reduction of the total energy occurs because $E < 0$ when the direction of \mathbf{S}' is parallel to that of \mathbf{H}'_E for $J' > 0$ and when the direction of \mathbf{S}' is antiparallel to that of \mathbf{H}'_E for $J' < 0$.

Here we consider the in-plane spin structure of MnCl₂-FeCl₃ GBIC. The FeCl₃ layers forming a honeycomb lattice is incommensurate with the MnCl₂ layers. For simplicity we assume that MnCl₂-FeCl₃ GBIC has a hcp-type structure as shown in Fig. 9. The open circles correspond to Mn²⁺ spins in the MnCl₂ layer, the closed circles correspond to Fe³⁺ spins in the FeCl₃ layer. Following Sakakibara's model, the in-plane spin structure of MnCl₂ layers of MnCl₂-FeCl₃ GBIC is considered to be quite different from that for stage-2 MnCl₂ GIC due to the effective interplanar exchange interaction J' between MnCl₂ layers and FeCl₃ layers. The change in the in-plane spin structure of MnCl₂ layers through J' may give rise to the increase of the intraplanar exchange interaction. Therefore the stable in-plane spin structure of MnCl₂ layers results from the competition between interplanar interaction energy and intraplanar interaction energy. This possible change of the in-plane spin structure for the MnCl₂ layers may give rise to a dominance of the ferromagnetic NN interaction J_0 over the antiferromagnetic second NN (J_1) and the third NN intraplanar exchange interactions (J_2), although this dominance of J_0 in MnCl₂-FeCl₃ GBIC cannot be proved from this simple model at all. Here we can only say that these competing interactions may be the origin of the ferromagnetic behavior in MnCl₂-FeCl₃ GBIC. The Curie-Weiss temperature Θ of this system is calculated as $\Theta = 2zJ_0S(S+1)/3 = 13.3$ K with $S = \frac{5}{2}$ and $z = 6$, where J_0 is the ferromagnetic NN interaction for stage-2 MnCl₂ GIC ($J_0 = 0.38$ K). This estimated value of Θ is found to be in good agreement with the experimental value of Θ (= 12.47 K). As described above, the positional relationship between Mn²⁺ ions and Fe³⁺ ions in the MnCl₂-FeCl₃ GBIC are much more complicated than that shown in Fig. 9. Due to this complicated nature it is difficult for us to elucidate the cause for the ferromagnetic behavior in MnCl₂-FeCl₃ GBIC.

C. Cluster glass phase for 0.7 < c ≤ 1

In the previous paper¹² we have presented a model of cluster glass phase for the explanation of the irreversible effect of SQUID magnetization in stage-2 Co_cMn_{1-c}Cl₂ GIC's with 0.8 ≤ c ≤ 1. The spins within small islands of the Co_cMn_{1-c}Cl₂ layers are ferromagnetically coupled below T_0 (= T_c), forming 2D ferromagnetic clusters. The spin directions of ferromagnetic clusters are frozen due to the frustrated interisland interactions consisting of

effective interplanar exchange interactions and dipole-dipole interaction between adjacent small islands. Similar types of cluster glass phase are also observed in $\text{Co}_c\text{Ni}_{1-c}\text{Cl}_2\text{-FeCl}_3$ GBIC's for $0 \leq c \leq 1$.⁹ The effective interplanar exchange interaction between adjacent $\text{Co}_c\text{Ni}_{1-c}\text{Cl}_2$ layers is enhanced by the intervening FeCl_3 layers through the interplanar interaction between $\text{Co}_c\text{Ni}_{1-c}\text{Cl}_2$ and FeCl_3 layers.

As described in Sec. IV B 1 the irreversible effect of magnetization for $\text{Co}_c\text{Mn}_{1-c}\text{Cl}_2\text{-FeCl}_3$ GBIC's with $0.7 \leq c < 1$ is different from that for $\text{Co}_c\text{Ni}_{1-c}\text{Cl}_2\text{-FeCl}_3$ GBIC's with $0 \leq c \leq 1$. The characteristic temperature T_0 seems to be independent of the concentration c for $\text{Co}_c\text{Mn}_{1-c}\text{Cl}_2\text{-FeCl}_3$ GBIC's ($T_0 \approx 9$ K), while T_0 coincides with T_c for $\text{Co}_c\text{Ni}_{1-c}\text{Cl}_2\text{-FeCl}_3$ GBIC's. This result suggests that the nature of cluster glass phase in $\text{Co}_c\text{Mn}_{1-c}\text{Cl}_2\text{-FeCl}_3$ GBIC's is different from that in $\text{Co}_c\text{Ni}_{1-c}\text{Cl}_2\text{-FeCl}_3$ GBIC's. In the $\text{Co}_c\text{Ni}_{1-c}\text{Cl}_2$ layers of $\text{Co}_c\text{Ni}_{1-c}\text{Cl}_2\text{-FeCl}_3$ GBIC's the resultant magnetic moment of the ferromagnetic clusters does not change too much with the concentration c because all the intraplanar interactions are ferromagnetic. The effect of 2D antiferromagnetic short-range spin order in the FeCl_3 layers on the cluster glass phase is almost concealed by the strong 2D ferromagnetic spin order in the $\text{Co}_c\text{Ni}_{1-c}\text{Cl}_2$ layers, leading to the cluster glass phase in the $\text{Co}_c\text{Ni}_{1-c}\text{Cl}_2$ layers only below T_c . In the $\text{Co}_c\text{Mn}_{1-c}\text{Cl}_2$ layers of $\text{Co}_c\text{Mn}_{1-c}\text{Cl}_2\text{-FeCl}_3$ GBIC's the spins within small islands are ferromagnetically coupled, forming ferromagnetic clusters at low temperatures. However, the resultant magnetic moment of the ferromagnetic clusters drastically decreases with decreasing concentration c due to the spin frustration effect arising from competing ferromagnetic and antiferromagnetic intraplanar interactions. The weak 2D ferromagnetic clusters in the $\text{Co}_c\text{Mn}_{1-c}\text{Cl}_2$ layers are effectively coupled to the 2D antiferromagnetic short-range spin order in the FeCl_3 layers through the interplanar interactions, leading to an enhanced spin frustration effect in the $\text{Co}_c\text{Mn}_{1-c}\text{Cl}_2$ layers for $T_c \leq T \leq T_0$.

VI. CONCLUSION

We have studied the magnetic properties of $\text{Co}_c\text{Mn}_{1-c}\text{Cl}_2\text{-FeCl}_3$ GBIC's by low-field SQUID magne-

tization, dc and ac magnetic-susceptibility measurements. These GBIC's with $0 \leq c \leq 0.1$ show a ferromagnetic behavior characterized by a positive Curie-Weiss temperature, an irreversible effect of SQUID magnetization, a broad peak of ac magnetic susceptibility at T_c , and a cusplike form of dc magnetic susceptibility at slightly lower temperature than T_c . This ferromagnetic behavior is explained in terms of either the ferromagnetic NN intraplanar interaction in the MnCl_2 layers or the spin frustration effect arising from competing Ising Fe^{2+} spins and $XY \text{Fe}^{3+}$ spins in the FeCl_3 layers. The GBIC's with $0.1 \leq c \leq 0.2$ show no magnetic phase transition at least above 1.5 K. The dc magnetic susceptibility of GBIC's with $0.25 \leq c \leq 0.7$ exhibits a broad peak around 3–4 K indicating that these systems undergo an antiferromagnetic phase transition at T_N associated with the growth of the antiferromagnetic long-range order in FeCl_3 layers. For $0.45 \leq c \leq 0.7$ the spin-glass-like phase also occurs below T_0 in the $\text{Co}_c\text{Mn}_{1-c}\text{Cl}_2$ layers due to the spin frustration effect arising from competing intraplanar exchange interactions. For $0.7 < c \leq 1$ there occurs a cluster glass phase below T_c where the spin directions of ferromagnetic clusters in the $\text{Co}_c\text{Mn}_{1-c}\text{Cl}_2$ layers are frozen due to the frustrated interisland interactions. Further studies including magnetic neutron scattering will be needed to understand in detail the magnetic phase transitions of $\text{Co}_c\text{Mn}_{1-c}\text{Cl}_2\text{-FeCl}_3$ GBIC's.

ACKNOWLEDGMENTS

We would like to thank H. Suematsu and Y. Hishiyama for providing us with high-quality single-crystal kish graphites, C. Vartuli, J. Morillo, T. Mellin, N. Inadama, J. Sciorra, and F. Khemai for their help with sample preparation of RMGIC's and GBIC's, M. D. Johnson for his help on dc magnetic-susceptibility measurements, and C. R. Burr for critical reading of this manuscript. The SQUID magnetization and electron microprobe measurements were carried out when we stayed at the Institute for Molecular Science in Japan. We are grateful to Y. Maruyama for giving us an opportunity to use the facilities. This work was supported by the National Science Foundation Grant No. DMR-9201656.

¹M. Suzuki, I. Oguro, and Y. Jinzaki, *J. Phys. C* **17**, L575 (1984).
²D. G. Rancourt, B. Hun, and S. Flandrois, *Ann. Phys.* **11**, Colloq. 2, Suppl. 2, 107 (1986).
³D. G. Rancourt, B. Hun, and S. Flandrois, *Can. J. Phys.* **66**, 776 (1988).
⁴I. Rosenman, F. Batallan, Ch. Simon, and L. Hachim, *J. Phys. (Paris)* **47**, 1221 (1986).
⁵S. Chehab, P. Biensan, J. Amiell, and S. Flandrois, *J. Phys. (France)* **I 1**, 537 (1991).
⁶S. Chehab, P. Biensan, S. Flandrois, and J. Amiell, *Phys. Rev. B* **45**, 2844 (1992).
⁷M. Suzuki, I. S. Suzuki, C. Vartuli, C. R. Burr, and Y. Maruyama, *Mol. Cryst. Liq. Cryst.* **245**, 93 (1994).

⁸S. Flandrois, P. Biensan, J. M. Louis, G. Chouteau, T. Roisnel, G. Andre, and F. Bouree, *Mol. Cryst. Liq. Cryst.* **245**, 105 (1994).
⁹I. S. Suzuki, C. Vartuli, C. R. Burr, and M. Suzuki, *Phys. Rev. B* **50**, 12 568 (1994).
¹⁰I. S. Suzuki, M. Suzuki, L. F. Tien, and C. R. Burr, *Phys. Rev. B* **43**, 6393 (1991).
¹¹M. Suzuki, I. S. Suzuki, F. Khemai, and C. R. Burr, *J. Appl. Phys.* **70**, 6098 (1991).
¹²I. S. Suzuki, M. Suzuki, and Y. Maruyama, *Phys. Rev. B* **48**, 13 550 (1993).
¹³Y. Kimishima, A. Furukawa, M. Suzuki, and H. Nagano, *J. Phys. C* **19**, L43 (1986).
¹⁴M. Matsuura, Y. Karaki, T. Yonezawa, and M. Suzuki, *Jpn.*

- J. Appl. Phys. **26**, Suppl. 26-3, 773 (1987).
- ¹⁵D. G. Wiesler, M. Suzuki, P. C. Chow, and H. Zabel, Phys. Rev. B **34**, 7951 (1986).
- ¹⁶K. Koga and M. Suzuki, J. Phys. Soc. Jpn. **53**, 786 (1984).
- ¹⁷M. Suzuki, S. M. Sampere, and K. Koga, Phys. Rev. B **39**, 6979 (1989).
- ¹⁸S. Miyashita and H. Shiba, J. Phys. Soc. Jpn. **53**, 1145 (1984).
- ¹⁹D. H. Lee, J. D. Joannopoulos, J. W. Negele, and D. P. Landau, Phys. Rev. Lett. **52**, 433 (1984).
- ²⁰M. Suzuki, I. S. Suzuki, D. G. Wiesler, and N. Rosov (unpublished).
- ²¹K. Ohhashi and I. Tsujikawa, J. Phys. Soc. Jpn. **36**, 422 (1974).
- ²²K. Ohhashi and I. Tsujikawa, J. Phys. Soc. Jpn. **36**, 980 (1974).
- ²³K. Ohhashi and I. Tsujikawa, J. Phys. Soc. Jpn. **37**, 63 (1974).
- ²⁴Y. S. Karimov, A. V. Zvarykina, and Y. N. Novikov, Sov. Phys. Solid State, **13**, 2388 (1972).
- ²⁵Ch. Simon, F. Batallan, I. Rosenman, J. Schweitzer, H. Lauter, and R. Vangelisti, J. Phys. (Paris) Lett. **44**, L641 (1983).
- ²⁶Y. Kimishima, H. Ikeda, A. Furukawa, and H. Nagano, J. Phys. Soc. Jpn. **55**, 3574 (1986).
- ²⁷K. Katsumata, J. Tuchendler, Y. J. Uemura, and H. Yoshizawa, Phys. Rev. **37**, 356 (1988).
- ²⁸M. Itoh, I. Yamada, M. Ishizuka, K. Amaya, T. Kobayashi, K. Koga, and K. Motoya, J. Phys. Soc. Jpn. **59**, 1792 (1990).
- ²⁹S. E. Millman and G. O. Zimmerman, J. Phys. C **16**, L89 (1983).
- ³⁰G. K. Wertheim, Solid State Commun. **38**, 633 (1981).
- ³¹D. Hohlwein, P. W. Readman, A. Chamberod, and J. M. D. Coey, Phys. Status Solidi B **64**, 305 (1974).
- ³²S. E. Millman, M. R. Corson, and C. R. Hoy, Phys. Rev. B **25**, 6595 (1982).
- ³³S. E. Millman and G. Kircznew, Solid State Commun. **44**, 1217 (1982).
- ³⁴F. Baron, S. Flandrois, C. Hauw, and J. Gaultier, Solid State Commun. **42**, 759 (1982).
- ³⁵T. Sakakibara, J. Phys. Soc. Jpn. **53**, 3607 (1984).